Grinding Behavior and Potential Beneficiation Options of Bauxite Ores

Evangelos Petrakis [1,*], **Georgios Bartzas** [2] **and Konstantinos Komnitsas** [1]

[1]   School of Mineral Resources Engineering, Technical University of Crete, University Campus, Kounoupidiana, 731 00 Chania, Greece; komni@mred.tuc.gr

[2]   School of Mining and Metallurgical Engineering, National Technical University of Athens, Zografos, 157 80 Athens, Greece; gbartzas@metal.ntua.gr

*   Correspondence: vpetraki@mred.tuc.gr; Tel.: +30-28210-37608

Abstract: This laboratory study investigates selective grinding and beneficiation options for a Greek bauxite ore. First, a series of batch grinding tests were carried out in order to investigate the grinding behavior of the ore and the effect of the material filling volume (f_c) on the distribution of aluminium- and iron-containing phases. Then, the ground ore was subjected to magnetic separation either as received or after reduction roasting in order to further explore potential beneficiation options. The results showed that grinding of the ore exhibits non-first order behavior, while the breakage rate varies with grinding time. Additionally, Al_2O_3 tends to concentrate in the coarser than 0.300 mm product fraction, while f_c 10% and 2 min of grinding time are considered optimum conditions for good distribution of Al_2O_3 and Fe_2O_3. When different product fractions were subjected to magnetic separation, it was seen that the non-magnetic product obtained from the 0.300–1.18 mm fraction was more rich in Al_2O_3. In this fraction, the Al_2O_3 content increased from 58 wt% in the feed to 67.9 wt%, whereas the Fe_2O_3 content decreased from 22.4 wt% in the feed to 13.5 wt%. When the ore was subjected to a two-step treatment, involving reduction roasting followed by magnetic separation, the Fe_2O_3 grade decreased from 20.8 to 5.1 wt%, but in this case the recovery was very low.

Keywords: bauxite ores; selective grinding; grinding kinetics; magnetic separation; reduction roasting

1. Introduction

Bauxite is an important rock which is used for the production of alumina of metallurgical or chemical grade through the Bayer process [1]. The global proven bauxite reserves are almost 30 billion tons and are located in Guinea (26.4%), Australia (19.2%), Brazil (12.1%) and Jamaica (7.1%), while other significant reserves exist in India, China, Greece and Suriname [2]. Bauxite deposits belong to two major types, namely the lateritic-type which account for 88% and the karst-type deposits which account for 12% of the world reserves. Lateritic-type are generally residual deposits derived from primary aluminosilicate rocks, while karst-type deposits are associated with carbonate rocks, where the bauxite body fills former karst cavities [3–5]. Karst-type deposits have different mineralogical composition compared to lateritic-type due to the presence of carbonates in the parent rock and the different weathering conditions [6].

In Greece, the major bauxite deposits were formed in the geotectonic zone of Parnassos-Ghiona, while economically important occurrences are found in Kallidromon, Iti, Nafpaktos, Smerna and Pylos [7,8]. The deposits of Parnassos-Ghiona are hosted within a carbonate sequence and belong to the Mediterranean karst bauxite belt. These allochthonous karst-type deposits are considered the most significant bauxite reserves in the European Union [9]; the estimated reserves are approximately 300 million metric tons—the 11th largest bauxite reserves globally [10]. In addition, Greece is the 12th

largest bauxite producer worldwide and a leading producer in the EU, with 1800 thousand metric tons production in 2017 [9,11].

Greek bauxite ores consist mainly of gibbsite [Al(OH)$_3$], diaspore [α-AlO(OH)] and/or boehmite [γ-AlO(OH)], while impurities such as kaolinite [Al$_2$Si$_2$O$_5$(OH)$_4$], hematite [Fe$_2$O$_3$], goethite [FeO(OH)], titanium oxide [TiO$_2$] and silicon oxide [SiO$_2$] are also present. The Al$_2$O$_3$ content varies between 49% and 65%, the Fe$_2$O$_3$ content between 18% and 24%, the CaO content between 0 and 5%, the SiO$_2$ content between 2% and 10%, the TiO$_2$ content between 0.5% and 3%, while the Cr and Ni content may be as high as 2000 mg/kg. Smaller amounts of magnesium, manganese, vanadium and gallium as well as other elements may be also found [12,13]. Greek bauxites are high grade compared to ores treated in several other parts of the word [14–16]. In Greece, 1.8 million tons are treated annualy mainly for the production of alumina (820,000 tons of which 480,000 tons are exported) and aluminium (185,000 tons of which 125,000 tons are exported). Minor quantities are used in cement plants, as a flux for the production of cast iron as well as for the production of rockwool and abrasive materials. It has been mentioned that in recent years, in order to reduce the underground mining cost, some quantities of tropical bauxites (0.4 million tons out of 1.8 million tons) have also been imported to and treated in Greece. The production of aluminum metal is generally accomplished by the Bayer process in which finely ground bauxite ore is digested in strong sodium hydroxide solution at a temperature range 100–250 °C [17]. The dissolved alumina is separated by physical means, such as settling and filtration, from the insoluble residue, known as "red mud" or recently as "bauxite residue". The amount of residue generated per ton of alumina produced, varies greatly depending on the type of bauxite used, from 0.3 tons for high grade bauxite to 2.5 tons for very low grade [18]. The bauxite residue mainly contains iron and silicon oxides, and other phases [19]. The Bayer process can economically produce alumina when Al$_2$O$_3$ to SiO$_2$ mass ratio in bauxite is greater than 10, while sintering or a combination of sintering and Bayer process can be used for ores with lower ratios. However, sintering is an energy-intensive process and increases the production cost of alumina [20–23].

Beneficiation is often considered for the upgrade of bauxite ores in order to also render them suitable for the refractory/ceramics industry [13,16]. Studies focusing on the removal of iron-bearing minerals include magnetic/gravimetric separation [24–26], reductive roasting followed by magnetic separation [17,22,27], froth flotation [28–30], leaching of iron oxides [31], chlorination followed by leaching [32] and microwave-magnetising roasting [33]. Other studies have attempted to upgrade bauxite ores through selective grinding by exploiting the different grindability between the minerals of interest, e.g., diaspore (6.5–7 Mohs hardness) and gangue minerals, e.g., kaolinite (2–2.5 Mohs hardness) and some other aluminosilicates [20,34].

Prior to any ore processing, grinding is the principal operation attracting particular attention due to the associated CO$_2$ emissions and the high energy consumption that affects the overall processing cost. Thus, in order to efficiently recover the economically valuable minerals an investigation of the ore behavior during grinding in relation to the operating parameters is required. Kinetic models which are based on two functions, namely the breakage rate and the breakage function are mainly used [35,36]. These models consider that grinding follows a first-order law as reported in previous studies [37,38]. However, deviations from first-order kinetics have been observed for several mineral phases indicating that the breakage rate varies with grinding time [39–41]. For non-first-order kinetics, the following Equation (1) proposed by Alyavdin can be used to describe the grinding process [42,43],

$$R_{i,t} = R_{0,t} \cdot e^{-K \cdot t^M} \tag{1}$$

where $R_{i,t}$ is the mass fraction of the mill hold-up that is of size i, $R_{0,t}$ is the mass fraction in the feed, K is the grinding rate constant, t is the grinding time and M is a constant depending on the material properties and grinding conditions.

The present laboratory study aims to investigate selective grinding and various beneficiation options for a Greek bauxite ore. First, selective grinding was carried out, through a series of batch

grinding tests, to elucidate the grinding behavior of the ore and assess the effect of the material filling volume in the mill. Second, the ore was subjected to magnetic separation to determine the distribution of Al- and Fe-containing phases. Third, reduction roasting followed by magnetic separation was investigated to enable the conversion of weak magnetic iron-bearing minerals to strong magnetic phases, i.e., magnetite or metallic iron, and further explore potential beneficiation options.

2. Materials and Methods

The bauxite ore used in the present study was provided by the mining company Delphi-Distomon S.A., which is one of the three Greek mining companies exploiting bauxite from the Parnassos-Ghiona zone, in central Greece. The ore is a typical red-brown (Fe-rich) bauxite composed of diaspore and boehmite as aluminum bearing mineral phases [44].

The received ore, approximately 150 kg, with a particle size of −30 mm was homogenized by the cone and quarter method, and a representative sample was crushed to −3.35 mm using a jaw crusher (Fritsch pulverisette 1, Fritsch GmbH, Idar-Oberstein, Germany). To determine the particle size distribution of the crushed products, the ore was wet screened at 0.106 mm, while the +0.106 mm fraction was dried and screened using a series of screens with an aperture ratio 2 to obtain six size fractions.

Chemical analyses were carried out by X-ray fluorescence (XRF) spectroscopy using a Bruker S2 Ranger Energy-dispersive ED-XRF (Bruker, Karlsruhe, Germany) spectrometer. The composition of major elements was also determined after complete dissolution of each fraction by acid digestion followed by atomic absorption spectroscopy (AAS). The differences between the two analytical approaches were marginal, so the results obtained by XRF analysis are presented in this study. The identification of the mineral phases was carried out by X-ray powder diffraction (XRD) using a Bruker-AXS D8 Advance type (Bruker) diffractometer. Quantitative phase analysis by the Rietveld method was also performed [45]. The microstructure of the ore and the products obtained after each treatment was examined by scanning electron microscopy (SEM) using a JEOL 6380LV microscope (JEOL Ltd., Tokyo, Japan) equipped with an Oxford INCA energy dispersive X-ray spectrometer (EDS). The thermal behavior of the ore was studied using a Perkin Elmer TGA-6/DTG differential thermogravimetric analyser (Perkin Elmer, Waltham, MA, USA). A mass of about 40 mg was heated to temperatures of up to 900 °C at a heating rate of 10 °C/min under pure N_2 atmosphere with a flow rate of 35 mL/min.

Three series of wet grinding tests were carried out in a laboratory ball mill (Sepor, Los Angeles, CA, USA) with an internal diameter of 204 mm using the crushed product −3.35 mm as feed material. Different grinding times, namely 2, 4, 8 and 12 min, were considered, while the grinding media used were stainless steel balls (ρ_b = 7.85 g/cm^3) of three different sizes, i.e., 40, 25.4, and 12.7 mm. In this test series, the total ball mass was kept constant at about 10 kg corresponding to ball filling volume J = 40%, while the material filling volume f_c varied between 5% and 15%. The interstitial filling U of the void spaces of the balls filled by material was calculated using Equation (2). The product obtained after each grinding period was wet sieved using a series of screens, namely 1.18, 0.300 and 0.075 mm. The mill specification data and test conditions are shown in Table 1.

$$U = \frac{f_c}{0.4 \cdot J} \tag{2}$$

The magnetic separation tests involved the treatment of three product fractions, namely −0.300 mm, 0.300–1.18 and 1.18–3.35, obtained after a specific grinding period. More specifically, the feed material in the mill, −3.35 mm, was ground using different material filling volumes f_c (5%, 10% and 15%) in order to obtain a product size of 50% passing 0.300 mm. Then, each grinding product was subjected to magnetic separation using three different types of magnetic separators, depending on the sample size fraction. The two coarse size fractions, namely 1.18–3.35 mm and 0.300–1.18 mm were treated with the use of a HS10 Perm Roll belt separator (Outokumpu Technology Inc., Jacksonville, FL, USA)

with magnetic field strength of 0.5 T and a Carpco model MIH(13)111-5 high intensity induced roll magnetic separator (Outokumpu Technology Inc., Carpco Division), respectively, while for the fine fraction −0.300 mm a Carpco model WHIMS 3x4L wet high intensity magnetic separator (Outokumpu Technology Inc., Carpco Division) was used. The magnetic separation process of the coarse fractions involved two stages, as seen in Figure 1a. According to the procedure followed, each fraction was subjected to magnetic separation and two products were obtained, namely a magnetic product (MI) and a non-magnetic product (NMI). After the first stage, the non-magnetic product was further treated in the same magnetic separator using a lower roll speed and a second magnetic product (MII) and a final non-magnetic (NMII) product were obtained. The 1.18–3.35 mm fraction was treated using 180 and 140 rpm roll speed in the first and second stage, respectively. For the 0.300–1.18 mm fraction the roll speed was maintained at 120 and 100 rpm in the first and second stage, respectively, while the magnet coil current was kept at 3 amp. The magnetic separation of the −0.300 mm fraction involved a strong magnetic field created within a cell containing iron spheroids which was placed between two poles. The process included three separation stages with decreasing magnet coil current ranging from 7 to 1.5 amp, corresponding to magnetic field strength between 0.8 and 0.3 T, as seen in Figure 1b. The feed to the magnetic separator was a slurry with a pulp density of 10 wt%. At each stage, the slurry was fed through the cell, the magnetic product was retained on the sphere-poles and the non-magnetic product was flushed through. Then, the magnetic field strength was removed and the obtained magnetic product was further treated using a lower coil current. Finally, three non-magnetic products, namely NMI, NMII, NMIII and one magnetic MIII were collected. All the products were filtered, oven dried at 105 °C for 24 h, weighed and characterized by XRF, XRD and SEM.

Table 1. Mill specification data and test conditions.

Item	Description	1st Series	2nd Series	3rd Series
Material	Bulk density (g/cm^3)	1.82	1.82	1.82
	Material filling volume, f_c (%)	5	10	15
	Interstitial filling, U (%)	31	63	94
	Pulp density, % (by weight)	60	60	60

Item	Description	In all series		
Mill	Diameter, D (cm)	20.4		
	Length, L (cm)	16.6		
	Volume, V (cm^3)	5423		
	Operational speed, N (rpm)	66		
	Critical speed, N_c (rpm)	93.7		
Balls	Diameter, d (mm)	40, 25.4, 12.7		
	Number	13, 51, 407		
	Weight (g)	3403.9, 3463.6, 3407		
	Density (g/cm^3)	7.85		
	Porosity (%)	40		
	Ball filling volume, J (%)	40		

The −0.300 mm grinding fraction obtained using material filling volume f_c = 10% in the mill was also subjected to reduction roasting followed by magnetic separation. Reduction roasting, which is an option used also for the treatment of bauxite residues, was carried out to facilitate reduction of iron minerals and production of magnetic phases, as indicated in earlier studies [46–48]. The reduction roasting was carried out in a Linn High Therm model HK 30 furnace (Linn High Therm GmbH, Eschenfelden, Germany) at 800 °C. A commercial activated-charcoal/carbon type Norit GAC 1240 purchased from Sigma–Aldrich (Sigma–Aldrich GmbH, Taufkirchen, Germany) was used as a reductant and Na_2CO_3 as the flux. The ore was mixed with carbon using carbon to bauxite (C/B) mass ratio 0.15, while the mass ratio of Na_2CO_3 to bauxite ore was maintained at 0.20. The parameters

used in this study, i.e., reductive roasting temperature and duration, C/B ratios and flux addition were based on previous tests carried out in the laboratory. The mixtures were placed in the furnace and heated to the required temperature at a heating rate of 17 °C/min under pure N_2 atmosphere with a flow rate of 200 mL/min. The duration of the reduction process was 1 h. Then, the samples were removed, cooled-down in a desiccator and stored in sealed plastic containers until characterization. The roasted samples were then subjected to the wet magnetic separation, as previously mentioned, by applying 3.5 amp coil current (0.6 T magnetic field strength) and two products, i.e., a magnetic and a non-magnetic one, were obtained.

(a)   (b)
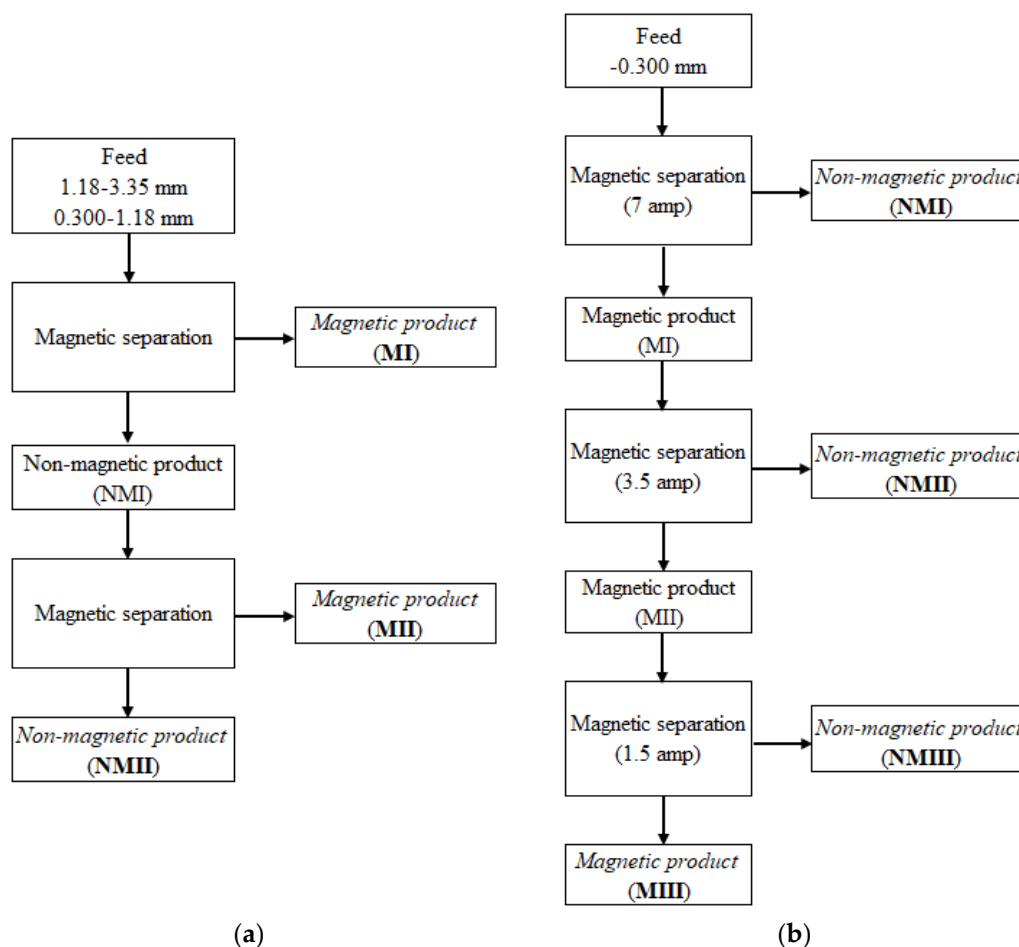
Figure 1. Schematic diagram of the process for the magnetic separation of (**a**) coarse fractions (1.18–3.35 mm and 0.300–1.18 mm) and (**b**) fine fraction (−0.300 mm).

3. Characterization of Bauxite Ore

Table 2 shows the main chemical composition, in the form of oxides, of each size fraction of the as received ore. The respective mass ratios of Al_2O_3 to SiO_2 and Al_2O_3 to Fe_2O_3 are also presented. It is observed that the main oxides present are Al_2O_3 and Fe_2O_3 assaying 57.95 and 22.39 wt%, respectively. The Al_2O_3 content in general decreases with decreasing size, while increased content of Fe_2O_3 is observed in the finer fractions. As a result, the mass ratio Al_2O_3/Fe_2O_3 decreases from 2.75 in the 1.70–3.35 mm fraction to 1.76 in the −0.106 mm fraction. The overall Al_2O_3/SiO_2 ratio is much greater (36.55) than 10 and thus, the bauxite is considered to be high-grade and can be processed directly by the Bayer process [49].

The XRD patterns of three representative different size fractions, namely 1.70−3.35 mm, 0.212−0.425 mm and −0.106 mm are shown in Figure 2. It is observed that the main aluminum containing phases present in the ore are diaspore [α-AlO(OH)] and boehmite [γ-AlO(OH)], while the

gangue minerals include hematite [Fe_2O_3], anatase [TiO_2] and kaolinite [$Al_2Si_2O_5(OH)_4$]. It is revealed from these patterns that in general the crystalline phases identified differ marginally between the different size fractions. However, the characteristic peaks of diaspore have higher intensity in the coarse fraction (1.70–3.35 mm), while the intermediate (0.212–0.425 mm) and fine (−0.106 mm) fractions contain more boehmite and hematite. In addition, kaolinite is more abundant in the fine fraction. These results are consistent with the quantitative phase analysis based on Rietveld method, which indicated that the diaspore content was 63 and 42 wt% in the coarse and fine fraction, respectively, while the hematite content was 10 and 14 wt%, respectively.

Table 2. Chemical composition of each bauxite fraction obtained after sieving.

Size (mm)	Mass (%wt)	Al_2O_3 (%wt)	Fe_2O_3 (%wt)	SiO_2 (%wt)	TiO_2 (%wt)	LOI [a] (%wt)	Al_2O_3/SiO_2	Al_2O_3/Fe_2O_3
1.70–3.35	38.52	58.76	21.34	1.68	3.90	5.1	34.98	2.75
0.850–1.70	20.93	59.45	21.38	1.43	3.81	2.7	41.51	2.78
0.425–0.850	14.69	58.33	22.32	1.44	3.90	1.9	40.63	2.61
0.212–0.425	9.95	58.37	22.38	1.41	3.94	1.3	41.35	2.61
0.106–0.212	6.66	57.65	23.00	1.64	3.99	0.9	35.23	2.51
−0.106	9.25	50.38	28.68	2.62	4.43	1.2	19.25	1.76
Total	100.0	57.95	22.39	1.65	3.94	13.0	36.55	2.62

[a] Loss on Ignition at 1050 °C for 3 h.
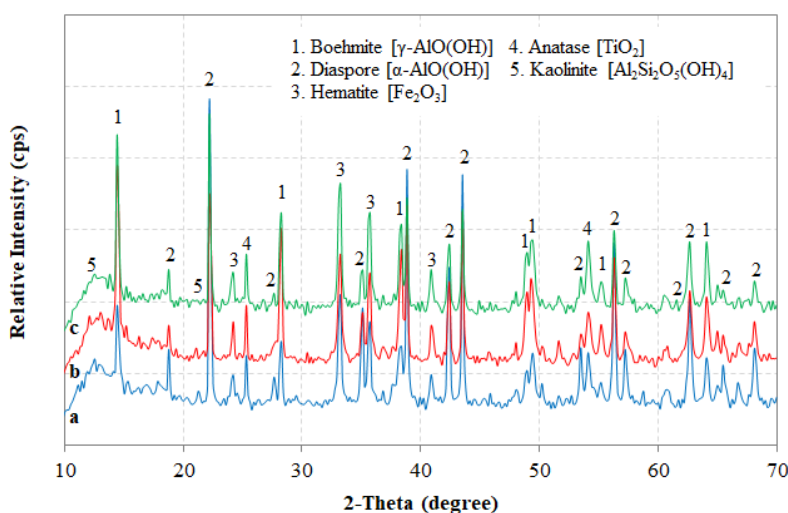
Figure 2. XRD patterns of three representative bauxite fractions obtained after sieving, namely (**a**) 1.70–3.35 mm fraction, (**b**) 0.212–0.425 mm fraction, and (**c**) −0.106 mm fraction.

Thermogravimetric analysis (TGA) and derivative thermogravimetric analysis (DTG) of the bauxite ore are presented in Figure 3. The TGA thermograms show a weight loss of about 2% up to 78 °C, which is attributed to the loss of the inherent moisture of the ore. After this temperature a three-stage weight loss was observed. The weight loss (~3%) detected in the 78–486 °C range can be attributed to the dehydroxylation of boehmite, while a sharp weight loss of 9% was observed at the 486–580 °C temperature range. This bigger weight loss is associated with the peak on DTG curve at 532 °C, which indicates the removal of the chemically bound water present in diaspore [50,51]. Dehydration and removal of the structural water of boehmite and kaolinite may also occur at this temperature range. However, due to the lower content of boehmite and kaolinite in the ore compared to diaspore, these effects overlap with the dehydration effect of diaspore [52]. The third stage of weight loss (~1.4%) is recorded in the range 580–900 °C and may be assigned to the release of CO_2 due to the decomposition of calcite. However, calcite was not detected by XRD and this may be due to fact that its content is below the detection limit (<2 wt%) of the instrument [53].
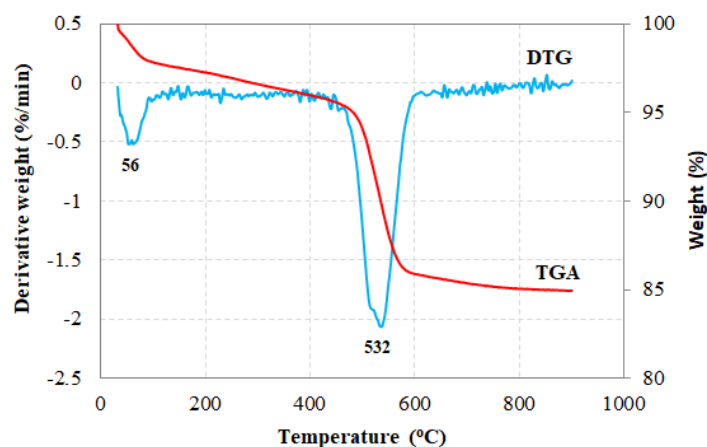
Figure 3. TGA and DTG curves of the bauxite ore.

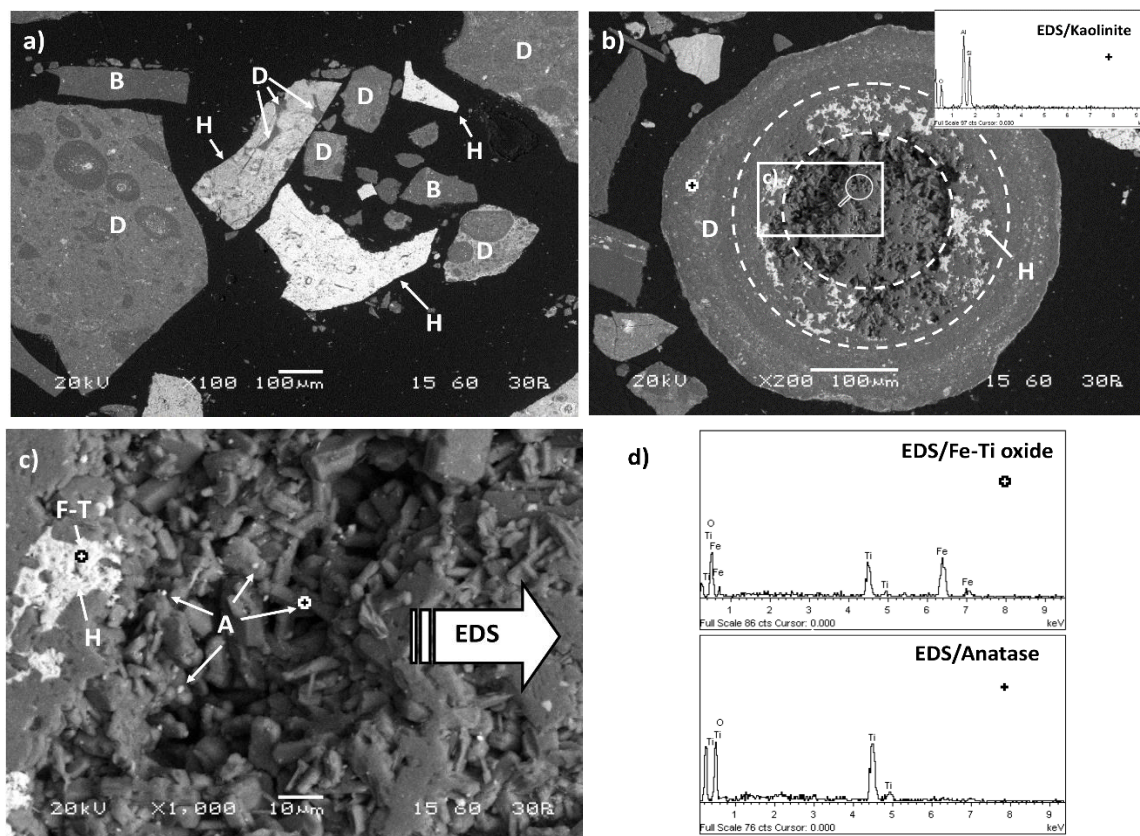SEM images of the bauxite ore (crushed product −3.35 mm) along with EDS composition data are shown in Figure 4a–d.

Figure 4. (**a**–**c**) Cross sectional SEM-backscattered electron (BSE) images of polished surfaces of bauxite ore (crushed product −3.35 mm). EDS spectra obtained in several spot locations (**b**–**d**) show the presence of oxide phases, the mineral formation of the bauxite clasts and mixed/intergrown oxides in the diasporic matrix (D: Diaspore; B: Boehmite; H: Hematite; A: Anatase; K: Kaolinite; F-T: Fe-Ti oxide).

Microscopic characterization of polished bauxite surfaces proved that the main Al-bearing and Fe-rich phases present in the ore are diaspore [α-AlO(OH)], boehmite [γ-AlO(OH)] and hematite [Fe_2O_3], respectively (Figure 4a). In accordance with the XRD results, remarkable minor quantities of anatase [TiO_2] and kaolinite [$Al_2Si_2O_5(OH)_4$] (mixed with Al-oxides) were also found in the diasporic

clasts of the ore (Figure 4b). More specifically, Figure 4c (zoom of rectangular area of Figure 4b) shows the presence of anatase that occurs in the form of individual microscale particles (<2 μm) widely dispersed within the diasporic core (center of the clast) as well as in the form of intergrown particles within the internal rings of hematite (inner-outer dashed line area) in the diasporic clast [11]. In this context, EDS point analyses confirmed the presence of Ti in the brightest particles, i.e., intergrown with hematite (Fe-Ti oxide) as well as individually (particles) within the diaspore core, while Si was detected in the gray region of the diasporic matrix due to kaolinite contribution (Figure 4b–d).

4. Results and Discussion

4.1. Kinetic Behavior of Grinding Process

The grinding behavior of the bauxite ore was evaluated by identifying the relationship between the remaining mass (%) fraction of each particle size vs. grinding time. Figure 5a shows, as an example, the experimental data obtained for four selected sizes, namely 0.600, 0.300, 0.150 and 0.075 mm when the material filling volume (f_c) was 5%. It is observed that the experimental data are expressed well by Equation (1) and thus, grinding of the ore exhibits non-first-order behavior and the grinding rate of each size fraction is time dependent. High values of correlation coefficient R^2, ranging from 0.996 to 1.0, were obtained for the different f_c values used. In general, the reduction rate of larger particle sizes is higher than that of smaller particles with increasing grinding time, indicating that larger particles are ground more efficiently. Figure 5b shows the fitting curves of the particle size 0.300 mm when Equation (1) was applied to the experimental data, for different f_c values (5%, 10% and 15%). It is apparent that the reduction rate for a specific particle size depents on the material filling volume f_c and thus the grinding rate and consequently the grinding efficiency increases with decreasing f_c. As can be seen in Table 3, which shows the calculated parameters K and M by fitting the Alyavdin equation to experimental data, the grinding rate constant K decreases from 0.206 to 0.043 when f_c increases from 5% to 15%. It is also seen that M values range between 0.780 and 1.084, confirming the non-first-order grinding behavior of the ore [37,41,54].
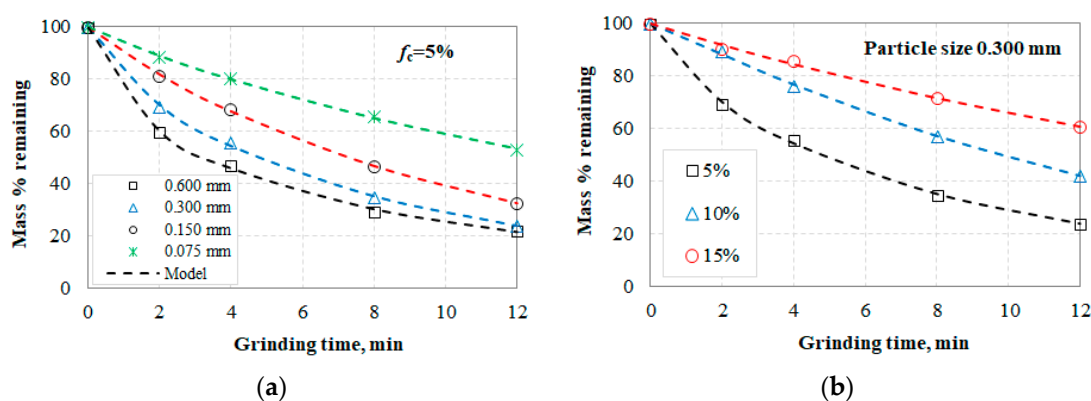
Figure 5. Remaining mass fraction (wt%) vs. grinding time for (**a**) four selected sizes when f_c = 5% and (**b**) particle size 0.300 mm when diferrent f_c values (5%, 10% and 15%) were used.

Table 3. Parameters of Alyavdin formula (Equation (1)) for particle size 0.300 mm at different f_c values.

Parameter	f_c = 5%	f_c = 10%	f_c = 15%
K	0.206	0.059	0.043
M	0.780	1.084	0.987
R^2 (adj.)	0.999	0.999	0.996

4.2. Al$_2$O$_3$ and Fe$_2$O$_3$ Content of the Selective Grinding Products

Figure 6 shows the Al$_2$O$_3$ and Fe$_2$O$_3$ content as well as the mass recovery (yield) in the product fractions (as cumulative oversize) after 2 min of grinding when the material filling volume (f_c) was 10%. It is seen that as size decreases the yield in the product coarser than this size increases. In light of this, mass recovery increases from 43.2 to 87.6 wt% when the product size decreases from 1.18 to 0.106 mm. With decreased product size the Fe$_2$O$_3$ grade of the coarser particles increased by 5.6 wt%, while the Al$_2$O$_3$ grade decreased slightly by 1.7 wt%, from 65 to 63.3 wt%. The results show that the content of Al$_2$O$_3$, which is mainly present in diaspore, increases slightly in coarser fractions, while Fe$_2$O$_3$ grade becomes higher in finer fractions indicating good selectivity during grinding. However, the mass recovery in coarser fractions and consequently the overall Al$_2$O$_3$ recovery is very low.
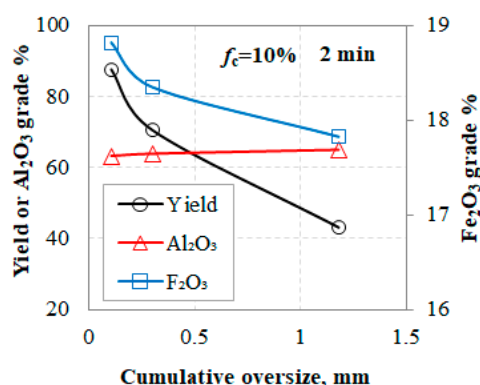
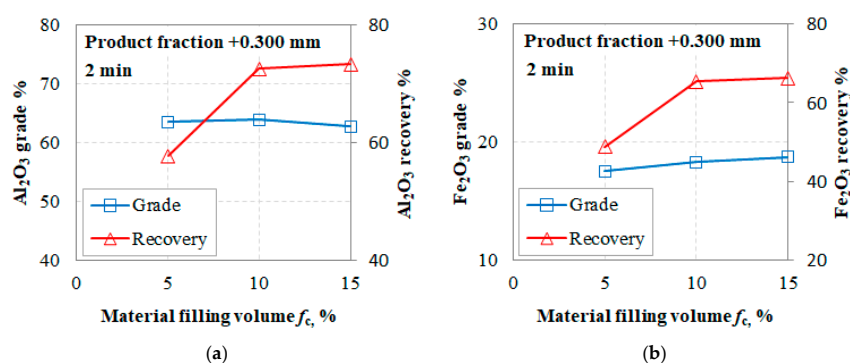**Figure 6.** Al$_2$O$_3$ grade, Fe$_2$O$_3$ grade and mass recovery (yield) in the cumulative oversize after 2 min of grinding and when f_c = 10%.

The effect of grinding time on Al$_2$O$_3$ grade and recovery for the product fractions coarser than 1.18 mm and 0.300 mm is presented in Figure 7a,b respectively. It is seen from Figure 7a that Al$_2$O$_3$ recovery in the product fraction coarser than 1.18 mm decreases from 45.2 to 21.8 wt% as grinding time increases from 2 to 12 min, respectively, while the Al$_2$O$_3$ grade remains almost constant, ~65 wt%, during grinding. Higher Al$_2$O$_3$ recovery can be achieved for the product fraction coarser than 0.300 mm, as seen in Figure 7b. In this context, Al$_2$O$_3$ recovery reaches almost 73 wt% after 2 min of grinding with a corresponding Al$_2$O$_3$ grade 64 wt%. At this grinding period, the Fe$_2$O$_3$ grade was 18.3 wt% and the corresponding recovery 65.4 wt%. Thus, better results can be obtained in terms of Al$_2$O$_3$ recovery for the product fraction coarser than 0.300 mm and after 2 min of grinding.

(a)   (b)
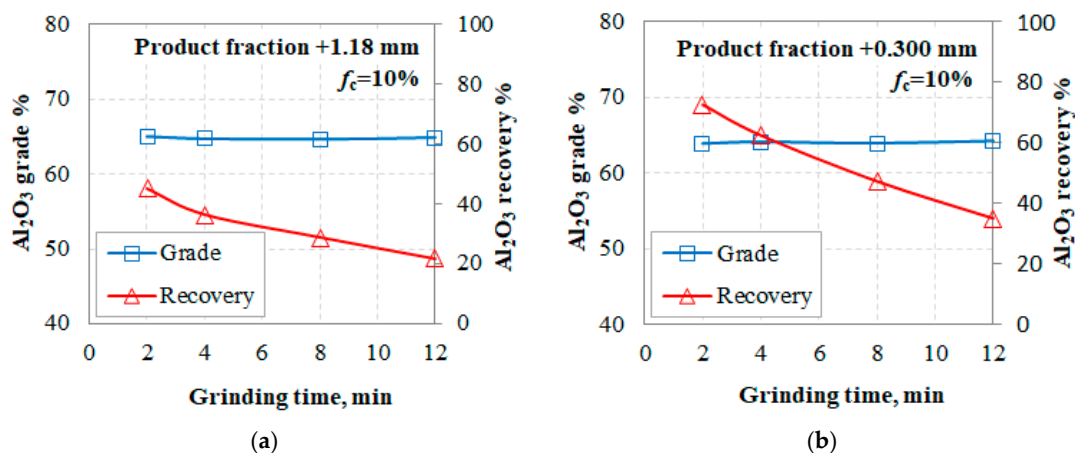
Figure 7. Effect of grinding time on Al$_2$O$_3$ grade and recovery for the product fraction coarser than (**a**) 1.18 mm and (**b**) 0.300 mm, when f_c = 10%.

Figure 8a presents the effect of material filling volume f_c (5%, 10% and 15%) on Al_2O_3 grade and recovery for the product fraction coarser than 0.300 mm after 2 min grinding. It is observed that Al_2O_3 grade increases marginally from 63.5 to 64 wt% with increasing f_c from 5% to 10% and then drops to 62.6 wt% when f_c was 15%. However, Al_2O_3 recovery increases significantly from 57.7% to 73% when f_c increases to 10% and reaches 73.4 wt% at f_c = 15%. Similar results were obtained for the Fe_2O_3 grade and recovery in the product fraction coarser than 0.300 mm, as seen in Figure 8b. Fe_2O_3 grade increased slightly from 17.6 to 18.7 wt% with increasing f_c to 15%, while its recovery reached 66.2 wt%. Based on these results, f_c = 10% can be considered as the optimum material volume in the mill for upgrading the bauxite ore during grinding. Under these conditions, the Al_2O_3 grade increased by 9.5 wt% compared with the raw ore, with corresponding recovery 73 wt%, while the Fe_2O_3 grade decreased by 18.3 wt% and its recovery was 65.4 wt%. It is worth mentioning that despite the fact that a higher grinding rate of the material is achieved when f_c = 5% (Table 3), the results in terms of Al_2O_3 grade and recovery are not satisfactory. Hence, the results of the present study show that the usual industrial practice of using higher milling rate does not necessarily result in efficient separation between the different minerals of interest present in ores or concentrates. Thus, detailed grinding kinetics analysis is required in order to determine the optimum grinding conditions that maximize the breakage rate of the minerals of interest, as for example diaspore in this case, while minimizing the respective rate of the impurities [55].

Figure 8. Effect of material filling volume f_c on (**a**) Al_2O_3 grade and recovery and (**b**) Fe_2O_3 grade and recovery for the product fraction coarser than 0.300 mm after 2 min of grinding.

Figure 9 presents the Al_2O_3 enrichment ratio (Al_2O_3 grade in the product: Al_2O_3 grade in the feed) for the cumulative oversize product after 2 min of grinding when different material filling volumes f_c were used. The results show that when the material filling volume f_c was 10%, in all cases a higher Al_2O_3 enrichment ratio was obtained, while the lowest enrichment ratio was achieved at f_c = 15%. The maximum ratio of 1.12 was achieved for the coarser than 1.18 mm product fraction with 65 wt% Al_2O_3 grade and corresponding recovery 45.2 wt%.
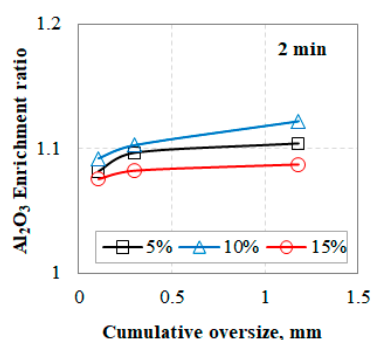
Figure 9. Al_2O_3 enrichment ratio in the cumulative oversize after 2 min of grinding when different material filling volumes f_c were used.

4.3. Magnetic Separation Efficiency on Bauxite

Figure 10a shows the Al_2O_3 grade in the magnetic separation products, namely MI, MII and NMII for the 1.18–3.35 and 0.300–1.18 mm fractions, when the material filling volume $f_c$ was 10%. The Al_2O_3 grade in the feed is also presented for comparison. As expected, the non-magnetic product (NMII) has higher Al_2O_3 grade compared to the magnetic one, i.e., MI and MII. The Al_2O_3 grade in this product, although higher than the one in the feed, does not exceed 66.3 wt%. The feed fraction has a great effect on the magnetic separation efficiency given that the non-magnetic product obtained from the 0.300–1.18 mm fraction is more rich in Al_2O_3 despite the fact that finer feed fractions contain less Al_2O_3. The non-magnetic product (NMII) contained 14.6–15.7 wt% Fe_2O_3 depending on the feed fraction tested, as seen in Figure 10b. Fe_2O_3 grade in this product corresponds to a 9.6 and 21.8 wt% reduction when the feed fraction used was 1.18–3.35 and 0.300–1.18 mm, respectively.
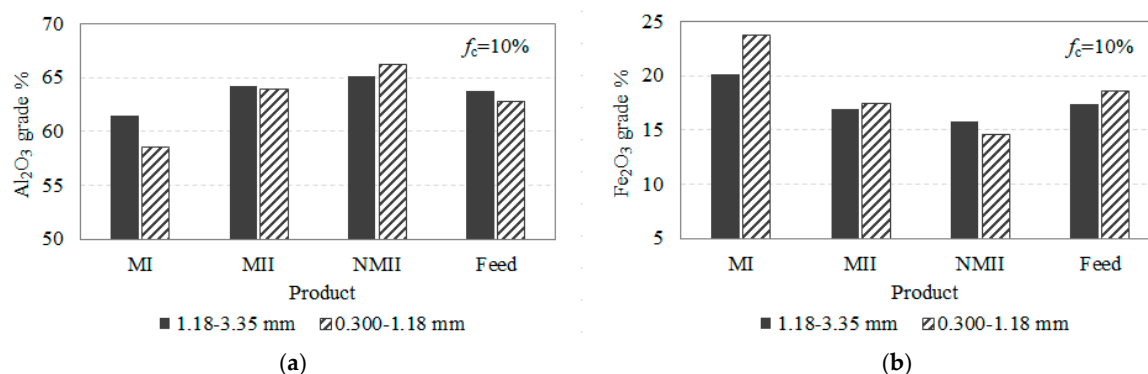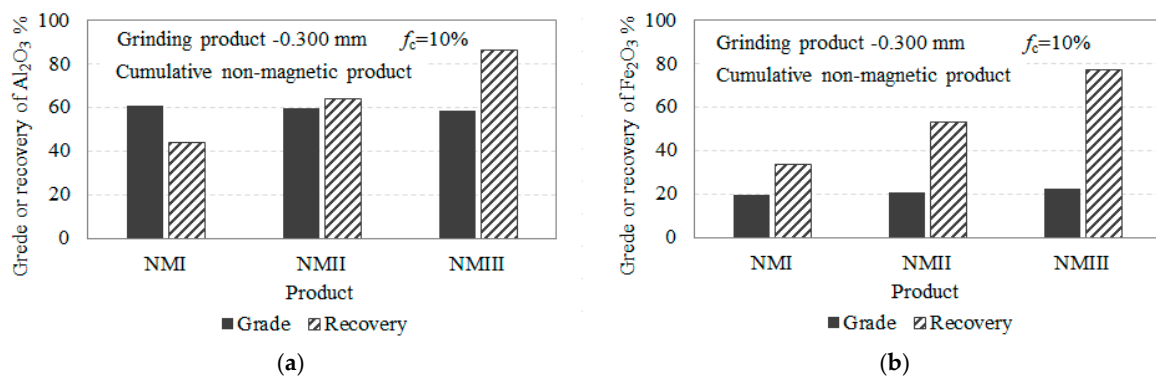

Figure 10. (**a**) Al_2O_3 grade and (**b**) Fe_2O_3 grade in the magnetic separation products for the 1.18–3.35 and 0.300–1.18 mm fractions, when the material filling volume f_c was 10%.

The effect of the material filling volume f_c on Al_2O_3 grade and recovery in the non-magnetic product NMII when the 0.300–1.18 mm fraction was subjected to magnetic separation is presented in Figure 11a. It is observed that the maximum Al_2O_3 grade and recovery, i.e., 67.85 and 47.8 wt%, respectively is achieved when f_c = 5% while at higher material filling volume (f_c = 10%) the respective quality slightly drops from 67.85 to 66.2 wt% and from 47.8 to 44.7 wt%. In addition, Al_2O_3 grade and recovery improve slightly when f_c increases from 10% to 15%. Under the optimum material filling volume (f_c = 5%) the Al_2O_3 grade is increased by 9.2 wt% by taking into account the grade in the 0.300–1.18 mm feed fraction. Under these conditions, the NMII product contains 13.51 wt% Fe_2O_3 corresponding to a decrease of 30.1 wt% compared to the feed fraction, as seen in Figure 11b. As material filling volume increases from 5 to 10 wt% the Fe_2O_3 grade also increases from 13.51 to 14.6 wt%, while the respective grade in the NMII product remains unchanged when f_c increases to 15%. The Fe_2O_3 recovery ranges between 30.5 and 32.7 wt% depending on the material filling volume tested.
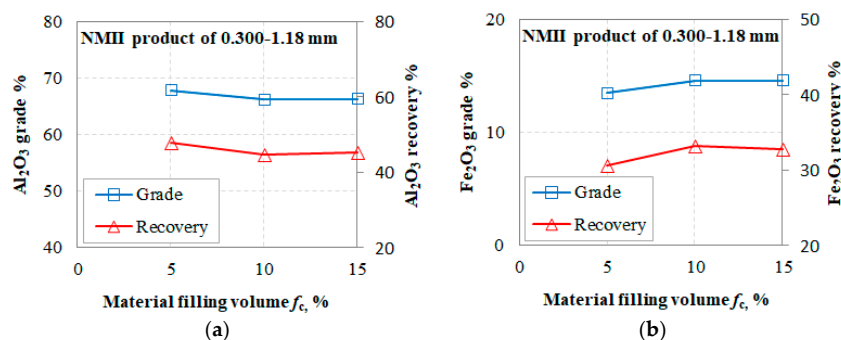
**Figure 11.** Effect of material filling volume f_c on (**a**) Al_2O_3 grade and recovery and (**b**) Fe_2O_3 grade and recovery in the NMII product when the 0.300–1.18 mm fraction was subjected to magnetic separation.

Figure 12a shows the Al_2O_3 grade and recovery in the cumulative non-magnetic product for the -0.300 mm fraction when the material filling volume f_c was 10%. It is seen that the Al_2O_3 recovery is continuously increasing from 44.2 to 86.3 wt% in the cumulative non-magnetic product, but the Al_2O_3 grade slightly decreased from 60.7 to 58.6 wt%. A similar trend was observed for Fe_2O_3 recovery which increased from 33.9 to 77.2 wt% by taking into account the same products (Figure 12b), indicating that the separation is not satisfactory, especially in the NMIII product, and a large amount of iron is distributed in the non-magnetic products. Thus, considering the Al_2O_3 and Fe_2O_3 recoveries in the products a two stage magnetic separation (cumulative NMII product) is considered adequate for better product quality. In addition, no significant differences in Al_2O_3, Fe_2O_3 grades and recoveries at different material filling volumes were observed. In light of this, Al_2O_3 grade and recovery in the cumulative NMII product varied between 59.4–60.3 wt% and 65–70.4 wt%, respectively, when f_c varied between 5% and 15%. This product contained about 21 wt% Fe_2O_3 with a recovery of about 56 wt%, which corresponds to a 10.9–14.1 wt% reduction depending on the grade of the feed fraction at each material filling volume.

(a) (b)

Figure 12. (**a**) Al_2O_3 grade and recovery and (**b**) Fe_2O_3 grade and recovery in the cumulative non-magnetic product for the -0.300 mm fraction when the material filling volume f_c was 10%.

Figure 13 presents the Al_2O_3 enrichment ratio for the non-magnetic products obtained after magnetic separation of different feed fractions for various material filling volumes f_c. The feed size indicated in this figure is the upper size of the tested size class. It is observed, for all material filling volumes used, that no major changes of the Al_2O_3 enrichment ratio occur. More specifically, the Al_2O_3 enrichment ratio increased slightly when the feed fraction increased from -0.300 to 0.300–1.18 mm and then dropped slightly for the coarse fraction 1.18–3.35 mm. The maximum ratio of 1.16 was achieved for the product fraction 0.300–1.18 mm when the material filling volume was 5%.
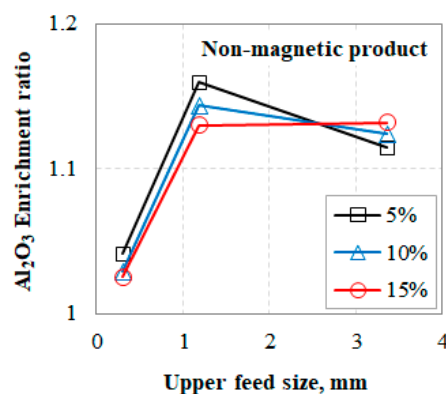
Figure 13. Al_2O_3 enrichment ratio in the non-magnetic products when different feed fractions were subjected to magnetic separation for various material filling volumes f_c.

The magnetic separation efficiency was also investigated using the Fuerstenau-II upgrading curves which relate recoveries of components in products [56,57]. Figure 14a shows the Fuerstenau-II upgrading plots of different feed fractions when the material filling volume f_c was 10%. It is shown that better separation of Al_2O_3 from Fe_2O_3 in the concentrate (non-magnetic product) is achieved when the 0.300–1.18 mm feed fraction was used, while the efficiency of magnetic separation is lower when the coarse fraction 1.18–3.35 mm was used. As shown in Figure 14b, which presents the effect of the material filling volume on the separation efficiency for the 0.300–1.18 mm fraction, slightly better results were obtained when the material filling volume was 15%. Overall, it can be concluded that in terms of Al_2O_3 and Fe_2O_3 recoveries in the non-magnetic products, better separation efficiency was achieved when the 0.300–1.18 mm fraction was subjected to magnetic separation using 15% material filling volume.
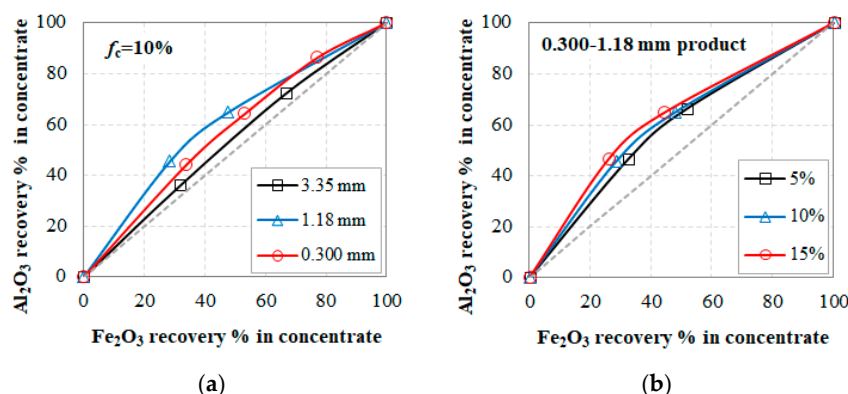
Figure 14. The Fuerstenau-II upgrading curves for different (**a**) feed fractions when f_c was 10% and (**b**) material filling volumes f_c when the 0.300–1.18 mm feed fraction was used.

4.4. Magnetic Separation Efficiency after Reduction Roasting of Bauxite

A reduction roasting–magnetic separation process can modify the distribution of aluminium and iron phases. In the reduction roasting process, weak magnetic iron-containing minerals such as hematite can be converted into strong ones, e.g., magnetite, or even metallic iron, which can be easily separated after magnetic separation [58–60]. Higher reductant dosage may result in the formation of magnetite. However, other studies indicated that the excess of coal affects negatively the magnetic separation efficiency, due to the further reduction of magnetite to wüstite (FeO) [17]. The following reactions can take place during reduction roasting,

$$3Fe_2O_3 + C \rightarrow 2Fe_3O_4 + CO \tag{3}$$

$$Fe_2O_3 + 3C \rightarrow 2Fe + 3CO \tag{4}$$

Additionally, in the presence of soda (Na_2CO_3), the main constituents of bauxite ore, e.g., Al_2O_3 and Fe_2O_3 may react according to Reaction (5), where *M* is a trivalent metal such as Al and Fe [61].

$$M_2O_3 + Na_2CO_3 \rightarrow 2NaMO_2 + CO_2 \tag{5}$$

Figure 15a shows the Al_2O_3 grade and recovery in the magnetic and non-magnetic products obtained after reduction roasting followed by magnetic separation. The non-magnetic product has higher Al_2O_3 grade compared to the magnetic one and reached 67.3 wt%, corresponding to an increase of 11.2 wt% compared to the feed fraction. However, its recovery is quite low and does not exceed the value of 35 wt%. On the other hand, the magnetic product contained 57.4 wt% Al_2O_3 with corresponding recovery 64.9 wt% which indicates the strong association of alumina containing phases with iron-bearing minerals. As seen in Figure 15b, which shows the Fe_2O_3 grade and recovery in the

magnetic separation products, Fe_2O_3 grade decreased to 5.1 wt% in the non-magnetic product from a feed fraction grade of 20.8 wt% (75.5% decrease) with corresponding recovery equals to 8 wt%. On the other hand, the magnetic product contained 28 wt% Fe_2O_3 with its recovery presenting very high value, i.e., 92.2 wt%. Overall, the results indicate that reduction roasting–magnetic separation is very efficient in reducing the iron content of bauxites. In cases where a lower grade bauxite was treated, unlike the one used in this study, this integrated approach could be beneficial in reducing the iron content (e.g., below 2–2.5 wt%), thus rendering bauxite suitable for other applications such as for the production of refractories and ceramics.
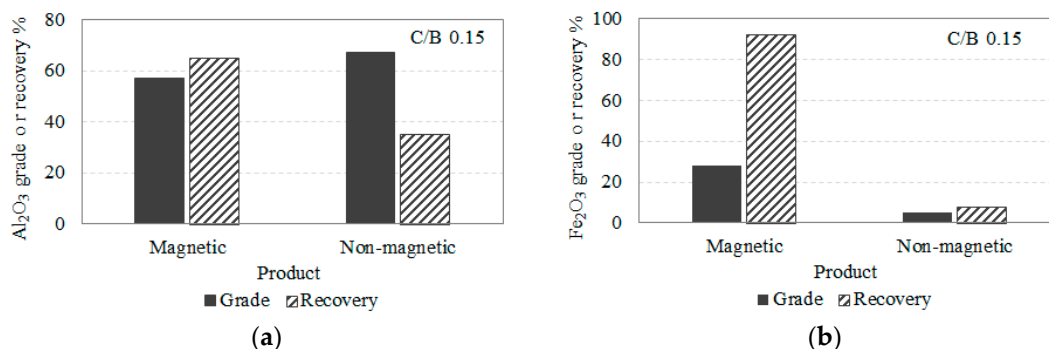
Figure 15. (**a**) Al_2O_3 grade and recovery and (**b**) Fe_2O_3 grade and recovery in the magnetic and non-magnetic products obtained after reduction roasting followed by magnetic separation.

4.5. Characterization of Magnetic Separation Products

Figure 16 shows the XRD patterns of the products, namely the non-magnetic product NMI and the magnetic product MIII obtained after magnetic separation of the −0.300 mm fraction, following the procedure seen in Figure 1b. The results indicate that the aluminum hydroxide phases, i.e., diaspore and boehmite present in this fraction have higher intensities in the non-magnetic product, while hematite is more abundant in the magnetic one. The characteristic peaks of anatase in the non-magnetic product were found to be more intense than those in the magnetic product, while no differences were observed for kaolinite in the two products examined. However, based on the results of the quantitative Rietveld analysis, it is revealed that kaolinite is slightly more abundant in the magnetic product indicating the poor liberation of this mineral phase which is associated with the iron-bearing phases prevailing in the ore.
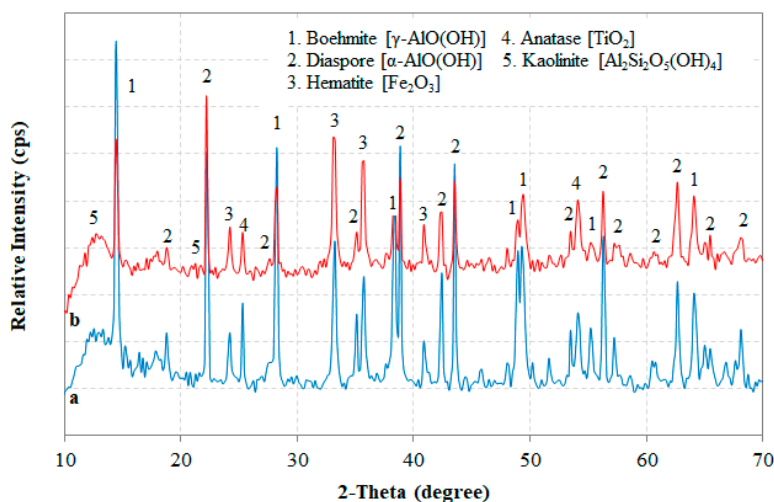
Figure 16. XRD patterns of (**a**) non-magnetic product NMI and (**b**) magnetic product MIII obtained after magnetic separation of the −0.300 mm fraction.

The XRD patterns of the non-magnetic and magnetic products obtained after reduction roasting followed by magnetic separation when carbon to bauxite (C/B) ratio was 0.15 are seen in Figure 17.
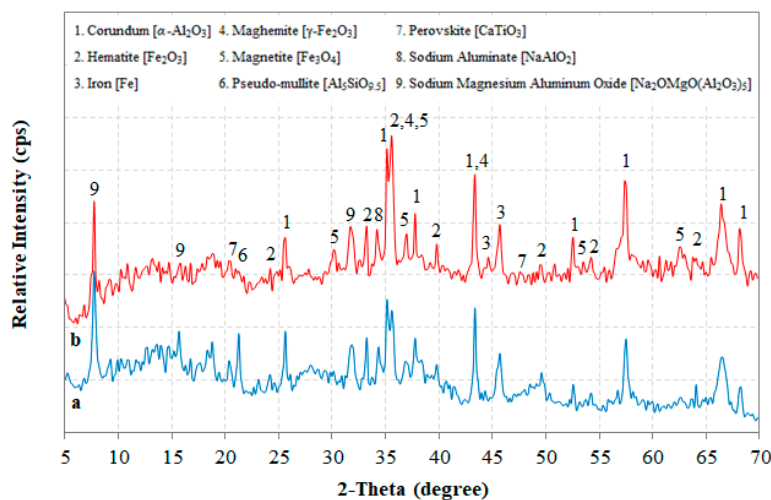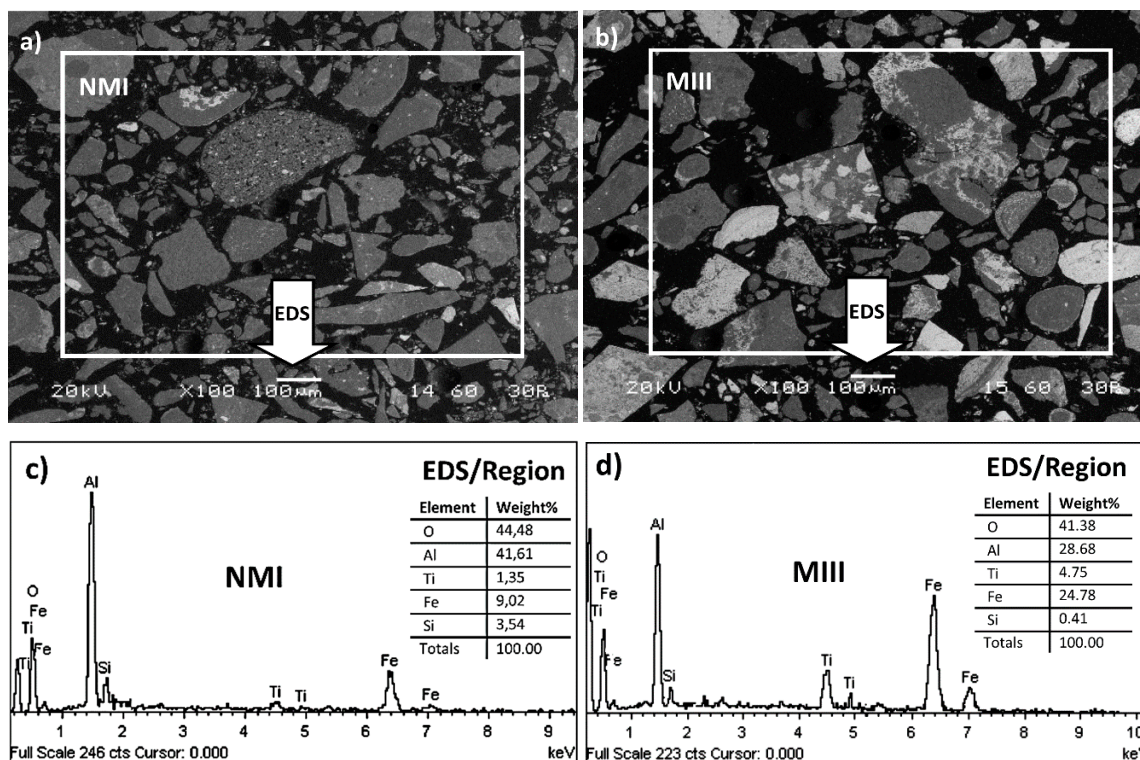

Figure 17. XRD patterns of (**a**) non-magnetic product and (**b**) magnetic product obtained after reduction roasting followed by magnetic separation when carbon to bauxite (C/B) ratio was 0.15.

It is seen from Figure 17 that the mineral phases present in the raw ore, i.e., diaspore, boehmite, anatase and kaolinite were not detected in the magnetic separation products, whereas less intense peaks of hematite are shown after reduction. Phase transformation took place during reduction roasting and the main minerals identified by XRD were corundum [α-Al$_2$O$_3$], hematite [Fe$_2$O$_3$], metallic iron [Fe], maghemite [γ-Fe$_2$O$_3$], magnetite [Fe$_3$O$_4$], pseudo-mullite [Al$_5$SiO$_{9.5}$], perovskite [CaTiO$_3$], sodium aluminate [NaAlO$_2$] and sodium magnesium aluminum oxide [Na$_2$OMgO(Al$_2$O$_3$)$_5$]. As a result, all alumina containing phases in the raw ore were transformed into corundum, sodium aluminate, sodium magnesium aluminum oxide and pseudo-mullite, while hematite was partially converted to magnetite, maghemite and metallic iron. According to previous studies, at ~780 °C diaspore and kaolinite transform into corundum and meta-kaolinite, respectively, whereas at temperature higher than 980 °C the formation of γ-Al$_2$O$_3$, amorphous SiO$_2$ and mullite is promoted [22]. In the temperature range of 200–250 °C, hematite transforms to magnetite, while the formation of metallic iron starts at temperatures higher than 900 °C [62]. In addition, despite the overlapping peaks of hematite, maghemite and magnetite at around 2-Theta = 35.6°, the remaining strongest peak of hematite at 2-Theta = 33.15° in the magnetic separation products reveals that this phase was not completely converted. The presence of perovskite in the roasted samples indicates that there was some amount of calcium in the raw ore, despite the fact that no Ca-bearing phases were identified by XRD. Comparing the magnetic separation products obtained after reduction roasting (Figure 17), it can be seen that the characteristic peaks of iron-bearing phases in the magnetic product have in general higher intensities than in the non-magnetic one, but no great difference was observed between the corundum peaks. Sodium aluminate, sodium magnesium aluminum oxide and pseudo-mullite although more abundant in the non-magnetic product are still present in the magnetic product indicating that the formed magnetic phases after reduction are associated with the non-magnetic ones. Thus, the complex mineralogy of the samples in combination with the incomplete hematite reduction results in a large amount of non-magnetic phases being trapped in the magnetic product.

SEM-BSE images of the products along with EDS analyses obtained after magnetic separation of the −0.300 mm fraction, namely the non-magnetic product NMI and the magnetic product MIII are shown in Figure 18a–d. As shown in Figure 18a, the bright particles corresponding to hematite almost disappeared in the non-magnetic product NMI and were limited to those Fe-rich particles (mostly Fe-Ti oxides) embedded in minor quantities in the diasporic matrix, thus their complete removal was difficult.

Figure 18. Cross-sectional SEM-BSE images of polished surfaces of (**a**) non-magnetic product NMI and (**b**) magnetic product MIII obtained after magnetic separation of the −0.300 mm fraction. EDS spectra obtained in regions (marked by white rectangle) of (**c**) non-magnetic product NMI and (**d**) magnetic product MIII confirm the metal content (Fe and Ti) increase in the MIII sample and the subsequent decrease of Al content.

On the other hand, microscopic characterization of the magnetic product MIII shows much greater bright area compared to the non-magnetic product NMI due to higher content in hematite, displayed both in the form of mixed and individual particles (Figure 18b). By comparing regional EDS spectra of non-magnetic product NMI and magnetic product MIII shown in Figure 18c,d, respectively, it was found that the metal content (Fe and Ti) of the MIII sample increased significantly; the Fe content increased from 9.02 to 24.78 wt%, the Ti content increased from 1.35 to 4.75 wt% while the Al content decreased from 41.61 to 28.68 wt%. This result is in accordance with XRD results shown in Figure 16 and suggests that the methodological procedure seen in Figure 1b effectively succeeded in separating the magnetic particles of the −0.300 mm fraction.

Figure 19 shows SEM-BSE images of the non-magnetic and magnetic products obtained after reduction roasting followed by magnetic separation when carbon to bauxite (C/B) ratio was 0.15. On the one hand, and in line with XRD results shown in Figure 17, SEM analysis along with EDS spectra data confirmed the depletion of the major Al-bearing phases present in the bauxite ore (feed material), namely diaspore and boehmite as well as gangue mineral phases such as anatase and kaolinite in both magnetic separation products; hematite was only detected in some places. On the other hand, bauxite particles have undergone excessive transformation during reduction roasting; this resulted in a micro-structure filled either with reduced particles entrapped in the matrix (non-magnetic product) or liberated/aggregated (magnetic product) as shown in Figure 19a,b–d, respectively.
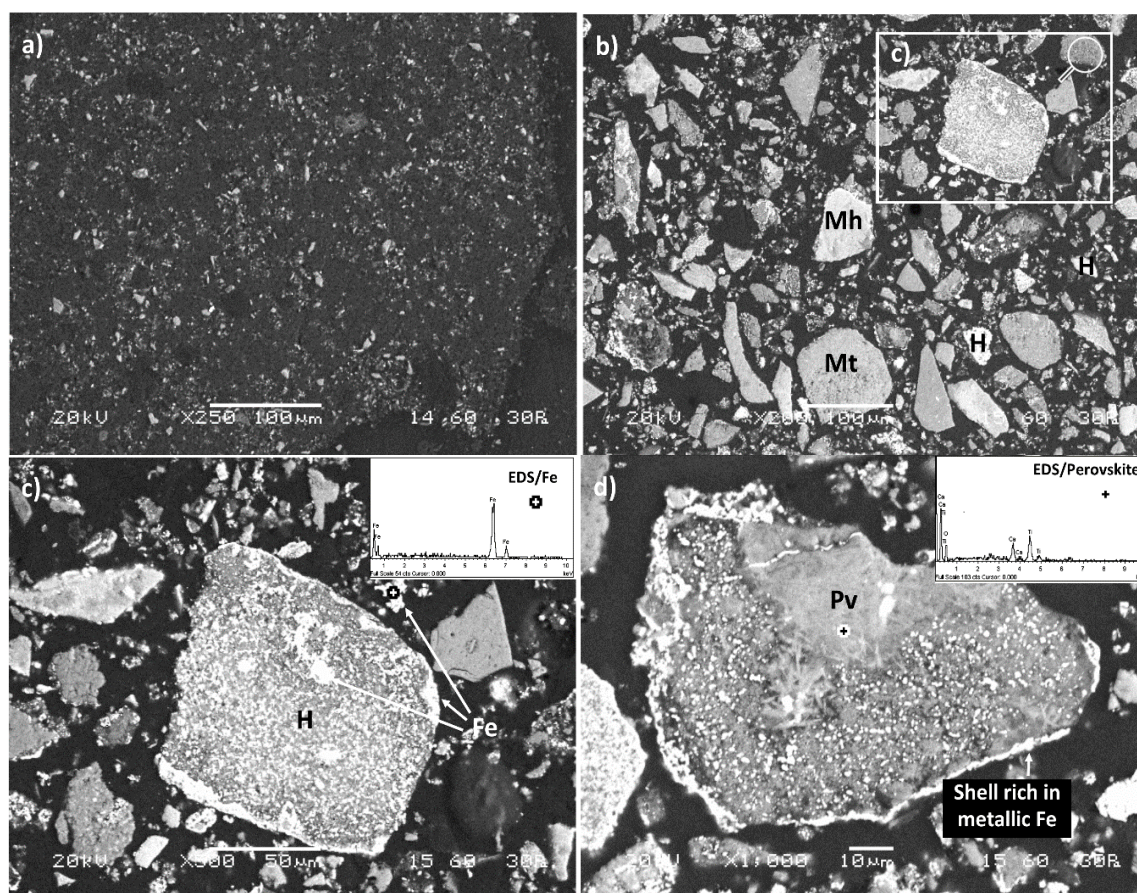
Figure 19. Cross sectional SEM-BSE images of polished surfaces of (**a**) non-magnetic product NMI and (**b–d**) magnetic product MIII obtained after reduction roasting followed by magnetic separation when carbon to bauxite (C/B) ratio was 0.15. EDS spectra obtained in several spot locations show the presence of newly formed metallic oxides (H: Hematite; Mt: Magnetite; Mh: Maghemite; Fe: Metallic iron; Pv: Perovskite).

In this context, and due to the addition of Na_2CO_3 during the roasting process, the transformation of Al-bearing phases into corundum, sodium aluminate, sodium magnesium aluminum oxide and pseudo-mullite is detected based on EDS point analyses conducted in both magnetic separation products. Reduction of hematite present in the bauxite ore and transformation into magnetite, maghemite and metallic iron is more clearly visible in the magnetic product as expected. More specifically, large particles of magnetite and maghemite (up to 100 µm) can be detected in the magnetic product while metallic iron is also formed in smaller particles (up to 5 µm). Figure 19c (zoom of rectangular area of Figure 19b) shows in detail the presence of metallic iron developed in the rim region/shell of hematite particles as well as aggregated and scattered in the matrix [63]. As can be seen in Figure 19d, perovskite [$CaTiO_3$] is the only Ti-rich oxide observed as needle-like infillings present at the internal space of the magnetic product thus indirectly confirming the calcium content in the bauxite ore (feed material).

Finally, the average chemical composition (in oxides) of the non-magnetic product NMI and the magnetic product MIII obtained after reduction roasting followed by magnetic separation based on EDS analyses conducted on respresentative regions of their polished surfaces are shown in Table 4. Results are given in comparison with the corresponding values obtained for the feed material (bauxite) and shown in Table 2. It is seen that the metal oxide content (Fe and Ti) of the non-magnetic product NMI decreased significantly; the Fe_2O_3 content decreased from 22.39 to 16.58 wt% , the TiO_2 content decreased from 3.94 to 1.14 wt% while the Al_2O_3 content increased from 57.25 to 68.23 wt% This result

suggests that the approach involving reduction roasting and magnetic separation has a synergistic and noticeable effect on bauxite beneficiation.

Table 4. Average chemical composition of the non-magnetic product NMI and the magnetic product MIII obtained after reduction roasting followed by magnetic separation in comparison with the feed material.

Sample	Al_2O_3 (wt%)	Fe_2O_3 (wt%)	SiO_2 (wt%)	TiO_2 (wt%)	LOI [a] (wt%)
NMI	68.23	16.58	2.32	1.14	9.73
MIII	58.05	27.25	0.89	5.14	7.67
Feed material (bauxite)	57.95	22.39	1.65	3.94	13.0

[a] Loss on Ignition.

5. Conclusions

The present experimental study aimed to optimize selective grinding of a Greek bauxite ore and explore potential beneficiation options that affect the distribution of Al- and Fe-containing phases.

Grinding kinetics showed that the breakage rate varies with grinding time, and therefore grinding of bauxite exhibits non-first-order behavior. The reduction rate depents on the particle size range as well as the material filling volume used in the mill. Coarse particles were ground more efficiently compared to the fine ones while the lower the material filling volume the higher was the reduction rate. Selective grinding showed that the content of Al_2O_3 increased slightly in the coarser fractions, while the Fe_2O_3 grade increased in the finer ones. However, the mass recovery in the coarser fractions and consequently the overall Al_2O_3 recovery was very low. Grinding time and material filling volume affected the grade and recovery of Fe_2O_3 and Al_2O_3 in the products. Best results were obtained for the coarser than 0.300 mm product fraction, after 2 min of grinding and when the material filling volume used was 10%. Under these conditions, the Al_2O_3 grade increased by almost 10% to 64 wt% with corresponding recovery 73 wt%, while the Fe_2O_3 grade decreased by 18.3% and its recovery was 65.4 wt%.

The magnetic separation of the products obtained after selective grinding showed that the feed fraction had significant effect on process efficiency. Thus, the non-magnetic product obtained from the 0.300–1.18 mm fraction was more rich in Al_2O_3 compared to 1.18–3.35 mm fraction, despite the fact that finer feed fractions contained less Al_2O_3. The maximum Al_2O_3 grade and recovery, i.e., 67.85 and 47.8 wt%, respectively, were obtained for a material filling volume of 5%. Under these conditions, the non-magnetic product contained 13.5 wt% Fe_2O_3, which corresponds to a decrease of 30.1%. The results of magnetic separation implemented after reduction roasting showed that a non-magnetic product containing 67.3 wt% Al_2O_3 but with quite low recovery (~35%) was obtained. In this product, Fe_2O_3 grade decreased by 75.5%, from 20.8 to 5.1 wt%, but in this case the corresponding recovery (8 wt%) was very low.

The results of this study indicate that reduction roasting followed by magnetic separation can be an effective approach for reducing the iron content of bauxites, but due to the complex mineralogy of the ores significant amounts of non-magnetic phases may be trapped in the magnetic fraction. To optimize grinding and roasting and maximize the efficiency and the cost effectiveness of the proposed integrated process, complete mineralogical and modelling studies are required to fully characterize the bauxite ore, select the proper mill and its best operating parameters and carry out reduction roasting at the correct temperature. In this case, improved beneficiation results are anticipated, especially for lower grade bauxite ores.

Author Contributions: Conceptualization, E.P. and K.K.; methodology, E.P., K.K. and G.B.; writing—original draft preparation, E.P. and G.B.; data analysis E.P., K.K. and G.B.; writing—review and editing, K.K. All authors have read and agreed to the published version of the manuscript.

Conflicts of Interest: The authors declare no conflict of interest.

References

1. Cardenia, C.; Balomenos, E.; Panias, D. Iron Recovery from Bauxite Residue Through Reductive Roasting and Wet Magnetic Separation. *J. Sustain. Metall.* **2019**, *5*, 9–19. [CrossRef]
2. Gibson, B.; Wonyen, D.G.; Chelgani, S.C. A Review of Pretreatment of Diasporic Bauxite Ores By Flotation Separation. *Miner. Eng.* **2017**, *114*, 64–73. [CrossRef]
3. Bogatyrev, B.A.; Zhukov, V.V.; Tsekhovsky, Y.G. Formation conditions and regularities of the distribution of large and superlarge bauxite deposits. *Lithol. Miner. Resour.* **2009**, *44*, 135–151. [CrossRef]
4. Ahmadnejad, F.; Zamanian, H.; Taghipour, B.; Zarasvandi, A.; Buccione, R.; Ellahi, S.S. Mineralogical and geochemical evolution of the Bidgol bauxite deposit, Zagros Mountain Belt, Iran: Implications for ore genesis, rare earth elements fractionation and parental affinity. *Ore Geol. Rev.* **2017**, *86*, 755–783. [CrossRef]
5. Vind, J.; Malfliet, A.; Blanpain, B.; Tsakiridis, P.E.; Tkaczyk, A.H.; Vassiliadou, V.; Panias, D. Rare Earth Element Phases in Bauxite Residue. *Minerals* **2018**, *8*, 77. [CrossRef]
6. Mucsi, G.; Csőke, B.; Solymár, K. Grindability characteristics of lateritic and karst bauxites. *Int. J. Miner. Process.* **2011**, *100*, 96–103. [CrossRef]
7. Laskou, M.; Andreou, G. Rare earth element distribution and REE-minerals from the Parnassos-Ghiona bauxite deposits, Greece. In Proceedings of the 7th Biennial SGA Meeting, Athens, Greece, 24–28 August 2003; Society for Geology Applied to Mineral Deposit: Genéve, Switzerland, 2003; pp. 89–92.
8. Eliopoulos, D.; Economou, G.; Tzifas, I.; Papatrechas, C. The potential of rare earth elements in Greece. In Proceedings of the ERES2014: First European Rare Earth Resources Conference, Milos, Greece, 4–7 September 2014.
9. U.S. Geological Survey. Bauxite and Alumina. Available online: http://minerals.usgs.gov/minerals/pubs/commodity/bauxite (accessed on 30 March 2020).
10. Laskou, M.; Economou-Eliopoulos, M.; Mitsis, I. Bauxite ore as an energy source for bacteria driving iron-leaching and bio-mineralization. *Hell. J. Geosci.* **2010**, *45*, 163–174.
11. Gamaletsos, P.N.; Godelitsas, A.; Kasama, T.; Church, N.S.; Douvalis, A.P.; Göttlicher, J.; Steininger, R.; Boubnov, A.; Pontikes, Y.; Tzamos, E.; et al. Nano-mineralogy and -geochemistry of high-grade diasporic karst-type bauxite from Parnassos-Ghiona mines, Greece. *Ore Geol. Rev.* **2017**, *84*, 228–244. [CrossRef]
12. Mutakyahwa, M.K.D.; Ikingura, J.R.; Mruma, A.H. Geology and geochemistry of bauxite deposits in Lushoto District, Usambara Mountains, Tanzania. *J. Afr. Earth Sci.* **2003**, *36*, 357–369. [CrossRef]
13. de Aquino, T.F.; Riella, H.G.; Bernardin, A.M. Mineralogical and physical-chemical characterization of a bauxite ore from Lages, Santa Catarina, Brazil, for refractory production. *Miner. Process. Extr. Metall. Rev.* **2011**, *32*, 137–149. [CrossRef]
14. Kumar, M.; Senapati, B.; Kumar, C.S. Beneficiation of high silica bauxite ores of India an innovative approach. In *Light Metals 2013*; The Minerals, Metals & Materials Series; Sadler, B.A., Ed.; Springer: Cham, Switzerland, 2016; pp. 187–190.
15. Rao, D.S.; Das, B. Characterization and beneficiation studies of a low grade bauxite ore. *J. Inst. Eng. (India): Ser. D* **2014**, *95*, 81–93. [CrossRef]
16. Sadler, L.Y.; Venkataraman, C. A process for enhanced removal of iron from bauxite ores. *Int. J. Miner. Process.* **1991**, *31*, 233–246. [CrossRef]
17. Pickles, C.A.; Lu, T.; Chambers, B.; Forster, J. A study of reduction and magnetic separation of iron from high iron bauxite ore. *Can. Metall. Q.* **2012**, *51*, 424–433. [CrossRef]
18. Komnitsas, K.; Bartzas, G.; Paspaliaris, I. Efficiency of limestone and red mud barriers: Laboratory column studies. *Miner. Eng.* **2004**, *17*, 183–194. [CrossRef]
19. Rivera, R.M.; Xakalashe, B.; Ounoughene, G.; Binnemans, K.; Friedrich, B.; Gerven, T.V. Selective rare earth element extraction using high-pressure acid leaching of slags arising from the smelting of bauxite residue. *Hydrometallurgy* **2019**, *184*, 162–174. [CrossRef]
20. Ou, L.M.; Feng, Q.M.; Zhang, G.F.; Chen, Y. Comminution property of bauxite and selective separation of Al and Si in bauxite. *Miner. Process. Extr. Metall.* **2008**, *117*, 179–184. [CrossRef]
21. Pehlivan, A.; Aydin, A.O.; Alp, A. Alumina extraction from low-grade diasporic bauxite by pyro- hydro metallurgical process. *SAÜ Fen Bilimleri Enstitüsü Dergisi* **2012**, *16*, 92–98. [CrossRef]

22. Gu, F.; Li, G.; Peng, Z.; Luo, J.; Deng, B.; Rao, M.; Zhang, Y.; Jiang, T. Upgrading Diasporic Bauxite Ores for Iron and Alumina Enrichment Based on Reductive Roasting. *J. Miner. Met. Mater. Soc. (TMS)* **2018**, *70*, 1893–1901. [CrossRef]

23. Marino, S.; Wang, X.; Lin, C.; Miller, J. The flotation of a gibbsite bauxite ore. In Proceedings of the 9th International Alumina Quality Workshop, Perth, Australia, 18–22 March 2012; pp. 345–350.

24. Bolsaitis, P.; Chang, V.; Schorin, H.; Aranguren, R. Beneficiation of ferruginous bauxite by high-gradient magnetic separation. *Int. J. Miner. Process.* **1981**, *8*, 249–263. [CrossRef]

25. White, J.C. Domestic saprolites as potential substitutes for refractory grade bauxite. *Ind. Eng. Chem. Res.* **1987**, *26*, 7–11. [CrossRef]

26. Kahn, H.; Tassinari, M.M.L.; Ratti, G. Characterization of Bauxite Fines Aiming to Minimize Their Iron Content. *Miner. Eng.* **2003**, *16*, 1313–1315. [CrossRef]

27. Rao, R.B.; Besra, L.; Reddy, B.R.; Banerjee, G.N. The effect of pretreatment on magnetic separation of ferruginous minerals in bauxite. *Magn. Electr. Sep.* **1997**, *8*, 115–123. [CrossRef]

28. Bittencourt, L.R.M.; Lin, C.L.; Miller, J.D. Flotation recovery of high-purity gibbsite concentrates from a Brazilian bauxite ore. In *Advanced Materials-Application of Mineral and Metallurgical Processing Principles*; Society of Mining Engineers of AIME: Salt Lake City, UT, USA, 1990; pp. 77–85.

29. Barbosa, F.D.M.; Bergerman, M.G.; Horta, D.G. Removal of iron-bearing minerals from gibbsitic bauxite by direct froth flotation. *Tecnol. Metal. Mater. Min.* **2016**, *13*, 106–112. [CrossRef]

30. Marino, S.L. The flotation of marginal Gibbstitic bauxite ores from Paragominas-Brazil. Master's Thesis, University of Utah, Salt Lake City, UT, USA, 2012.

31. Patermarakis, G.; Paspaliaris, Y. The leaching of iron oxides in boehmitic bauxite by hydrochloric acid. *Hydrometallurgy* **1989**, *23*, 77–90. [CrossRef]

32. Szabo, I.; Ujhidy, A.; Jelinko, R.; Vassanyi, R.I. Decrease of iron content of bauxite through high-temperature chlorination. *Hung. J. Ind. Chem.* **1989**, *17*, 465–475.

33. Ofori-Sarpong, G.; Abbey, C.E.; Asamoah, R.K.; Amankwah, R.K. Bauxite enrichment by microwave-magnetising roasting using sawdust as reducing agent. *Am. J. Chem. Eng.* **2014**, *2*, 59–64. [CrossRef]

34. Zhu, Y.; Han, Y.; Tian, Y.; Hong, W. Medium Characteristics on Selective Grinding of Low grade Bauxite. *Adv. Mater. Res.* **2010**, *158*, 159–166. [CrossRef]

35. Herbst, J.A.; Fuerstenau, D.W. Scale-up procedure for continuous grinding mill design using population balance models. *Int. J. Miner. Process.* **1980**, *7*, 1–31. [CrossRef]

36. Austin, L.G.; Klimpel, R.R.; Luckie, P.T. *Process Engineering of Size Reduction: Ball Milling*; SME–AIME: New York, NY, USA, 1984.

37. Petrakis, E.; Stamboliadis, E.; Komnitsas, K. Identification of optimal mill operating parameters during grinding of quartz with the use of population balance modelling. *KONA Powder Part. J.* **2017**, *34*, 213–223. [CrossRef]

38. Katubilwa, F.M.; Moys, M.H. Effect of ball size distribution on milling rate. *Miner. Eng.* **2009**, *22*, 1283–1288. [CrossRef]

39. Rajamani, R.K.; Guo, D. Acceleration and deceleration of breakage rates in wet ball mills. *Int. J. Miner. Process.* **1992**, *34*, 103–118. [CrossRef]

40. Bilgili, E.; Scarlett, B. Population balance modeling of non-linear effects in milling processes. *Powder Technol.* **2005**, *153*, 59–71. [CrossRef]

41. Petrakis, E.; Karmali, V.; Bartzas, G.; Komnitsas, K. Grinding kinetics of slag and effect of final particle size on the compressive strength of alkali activated materials. *Minerals* **2019**, *9*, 714. [CrossRef]

42. Harris, C.C. The Alyavdin-Weibull Plot of Grinding Data and the Order of Kinetics. *Powder Technol.* **1973**, *7*, 123–127. [CrossRef]

43. Beke, B. *The Process of Fine Grinding*; Dr. W. Junk Publishers: The Hague, The Netherlands, 1981.

44. Gamaletsos, P.; Godelitsas, A.; Kasama, T.; Kuzmin, A.; Lagos, M.; Mertzimekis, T.J.; Göttlicher, J.; Steininger, R.; Xanthos, S.; Pontikes, Y.; et al. The role of nano-perovskite in the negligible thorium release in seawater from Greek bauxite residue (red mud). *Sci. Rep.* **2016**, *6*, 21737. [CrossRef]

45. Young, R.A. *The Rietveld Method*; Oxford University Press: Oxford, UK, 1993.

46. Smith, P. The processing of high silica bauxites—Review of existing and potential processes. *Hydrometallurgy* **2009**, *98*, 162–176. [CrossRef]

47. Rai, S.; Nimje, M.T.; Chaddha, M.J.; Modak, S.; Rao, K.R.; Agnihotri, A. Recovery of iron from bauxite residue using advanced separation techniques. *Miner. Eng.* **2019**, *134*, 222–231. [CrossRef]

48. Deng, B.; Si, P.; Bauman, L.; Luo, J.; Rao, M.; Peng, Z.; Jiang, T.; Li, G.; Zhao, B. Photocatalytic activity of CaTiO$_3$ derived from roasting process of bauxite residue. *J. Clean. Prod.* **2020**, *244*, 118598. [CrossRef]

49. Yılmaz, K.; Birol, B.; Sarıdede, M.N.; Yiğit, E. Pre-Beneficiation of Low Grade Diasporic Bauxite Ore by Reduction Roasting. World Academy of Science, Engineering and Technology. *Int. J. Chem. Mol. Nucl. Mater. Metall. Eng.* **2015**, *9*, 1075–1078.

50. Kloprogge, J.T.; Ruan, H.D.; Frost, R.L. Thermal decomposition of bauxite minerals: Infrared emission spectroscopy of gibbsite, boehmite and diaspore. *J. Mater. Sci.* **2002**, *37*, 1121–1129. [CrossRef]

51. Laskou, M.; Margomenou-Leonidopoulou, G.; Balek, V. Thermal characterization of Bauxite samples. *J. Therm. Anal. Calorim.* **2006**, *84*, 141–145. [CrossRef]

52. Ostojić, G.; Lazić, D.; Škundrić, B.; Škundrić, J.P.; Sladojević, S.; Kešelj, D.; Blagojević, D. Chemical-mineralogical characterization of bauxites from different deposits. *Contemp. Mater.* **2014**, *1*, 84–94.

53. Castaldi, P.; Silvetti, M.; Enzo, S.; Deiana, S. X-ray diffraction and thermal analysis of bauxite ore-processing waste (red mud) exchanged with arsenate and phosphate. *Clays Clay Miner.* **2011**, *59*, 189–199. [CrossRef]

54. Fuerstenau, D.W.; Phatak, P.B.; Kapur, P.C.; Abouzeid, A.-Z.M. Simulation of the grinding of coarse/fine (heterogeneous) systems in a ball mill. *Int. J. Miner. Process.* **2011**, *99*, 32–38. [CrossRef]

55. Petrakis, E.; Karmali, V.; Komnitsas, K. Factors affecting nickel upgrade during selective grinding of low-grade limonitic laterites. *Miner. Process. Extr. Metall. Trans. Inst. Min. Metall.* **2018**. [CrossRef]

56. Fuerstenau, D.W.; Sastry, K.V.S.; Hanson, J.S.; Narayanan, K.S.; Urbina, R.H.; Diao, J.; Chen, W. *Coal Surface Control for Advanced Fine Coal Flotation*; Project No. DE-AC22-88PC88878, Final Report; University of California: Berkeley, CA, USA; University of Utah: Salt Lake City, UT, USA; Columbia University: New York, NY, USA; Praxis Engineers: Milpitas, CA, USA, 1992.

57. Drzymala, J.; Ahmed, H.A.M. Mathematical equations for approximation of separation results using the Fuerstenau upgrading curves. *Int. J. Miner. Process.* **2005**, *76*, 55–65. [CrossRef]

58. Li, X.; Xiao, W.; Liu, W.; Liu, G.; Peng, Z.; Zhou, Q.; Qi, T. Recovery of alumina and ferric oxide from Bayer red mud rich in iron by reduction sintering. *Trans. Nonferrous Met. Soc. China* **2009**, *19*, 1342–1347. [CrossRef]

59. Ravisankar, V.; Venugopal, R.; Bhat, H. Investigation on beneficiation of goethite-rich iron ores using reduction roasting followed by magnetic separation. *Miner. Process. Extr. Metall.* **2017**. [CrossRef]

60. Chun, T.J.; Zhu, D.Q.; Pan, J. Simultaneously roasting and magnetic separation to treat low grade siderite and hematite ores. *Miner. Process. Extr. Metall. Rev.* **2015**, *4*, 223. [CrossRef]

61. Kaußen, F.K.; Friedrich, B. Methods for Alkaline Recovery of Aluminum from Bauxite Residue. *J. Sustain. Metall.* **2016**. [CrossRef]

62. Jang, K.-O.; Nunna, V.R.M.; Hapugoda, S.; Nguyen, A.V.; Bruckard, W.J. Chemical and mineral transformation of a low grade goethite ore by dehydroxylation, reduction roasting and magnetic separation. *Miner. Eng.* **2014**, *60*, 14–22. [CrossRef]

63. Samouhos, M.; Taxiarchou, M.; Tsakiridis, P.E.; Potiriadis, K. Greek "red mud" residue: A study of microwave reductive roasting followed by magnetic separation for a metallic iron recovery process. *J. Hazard. Mater.* **2013**, *254*, 193–205. [CrossRef] [PubMed]